Suplemento de la Revista Mexicana de Física **2** (1) 81–86 JANUARY-MARCH 2021

Analysis of whispering gallery modes resonators: wave propagation and energy balance models

E. Rivera-Pérez[a], A. Díez[b], J. L. Cruz[b], E. Silvestre[b], and M. V. Andrés[b,*]

[a] *Departamento de Física, Universidad de Guanajuato, Loma del Bosque 103, 37150, México.*
[b] *Universidad de Valencia, ICMUV, c/Dr. Moliner 50, Burjassot, 46100 Valencia, Spain.*
[*] *e-mail: miguel.andres@uv.es*

Received 8 December 2020; accepted 21 December 2020

Electromagnetic whispering gallery modes (WGM) are surface waves guided by the curvature of an interface. Microspheres, microdisks, and microcylinders –for example, standard optical fibers– are high quality microresonators for the WGM. In fact, they can be regarded as compact and small ring resonators. Here, we present a comparison between wave propagation and energy balance models, establishing the equivalence and discussing the basic characteristics of these two complementary approaches.

Keywords: Microresonators; optical microcavities; whispering gallery modes; microfibers; opticla fibers.

PACS: 42.81; 42.82

1. Introduction

Microresonators based on WGM exhibit high Q factors, probably the highest ever reported, which makes them particularly attractive for different applications as narrowband spectral filtering [1], single-frequency lasers [2], generation of frequency combs [3], and sensing [4]. In particular, azimuthal WGM resonances of optical fibers have been demonstrated to be useful for the characterization of optical fibers: thermal effects in active fibers [5], fiber diameter fluctuations [6,7], UV-induced losses [8], and Pockels' coefficients [9].

Different approaches have been developed for the theoretical analysis of WGM resonators. On the one hand, WGM resonators can be regarded as compact and small interferometers and can be described in terms of the amplitude and phase of the electromagnetic waves that propagate in the device. On the other hand, being a resonator, one can formulate a differential equation that describes the energy balance between the WGM and the input and output waves. We will refer to the first one as a wave propagation model (WPM) and the second as an energy balance model (EBM).

The WPM is closely related to the approach that is commonly used for the description of fiber interferometers as the analysis developed by Evgeny Kuzin for the fiber Sagnac interferometer [10]. The same approach has been used for the study of the Mach-Zehnder interferometers [11] and ring resonators [12]. A microresonator coupled to an optical fiber via the evanescent fields of microfiber can be regarded as a tiny optical fiber ring resonator. The EBM [13,14] is analogous to the laser models based on time dependent rate equation where the spatial variation of the fields is not included [15]. Here, we will establish the equivalence between WPM and EBM and a comparison with experimental data will be also discussed.

2. The wave propagation model (WPM)

Figure 1 illustrates the system that we are going to study, and it also includes two scanning electron microscope (SEM) images of representative WGM resonators. In principle, we assume that the cross-section of the microresonator is a perfect circle that is coupled to a microfiber via evanescent fields. The input wave with amplitude E_i will be, in most cases, the fundamental mode of a microfiber. The coupling between the input wave and the resonator is modeled with a four ports coupler defined by the matrix:

$$\begin{pmatrix} E_t \\ E_{ccw} \end{pmatrix} = \begin{pmatrix} \sqrt{1-\eta^2} & j\eta \\ j\eta & \sqrt{1-\eta^2} \end{pmatrix} \begin{pmatrix} E_i \\ E'_{ccw} \end{pmatrix}, \quad (1)$$

where E_t is the amplitude of the transmitted wave in the microfiber, E_{ccw} is the amplitude of the counter-clockwise WGM at the coupling point, E'_{ccw} is the amplitude of the WGM at the entrance of the coupling region – *i.e.*, E'_{ccw} is E_{ccw} after propagating one trip along the surface of the microresonator–, η is the coupling coefficient and $j \equiv \sqrt{-1}$.

The relationship between E'_{ccw} and E_{ccw} is determined by an overall transmission factor $f(f < 1)$ and a phase ϕ de-

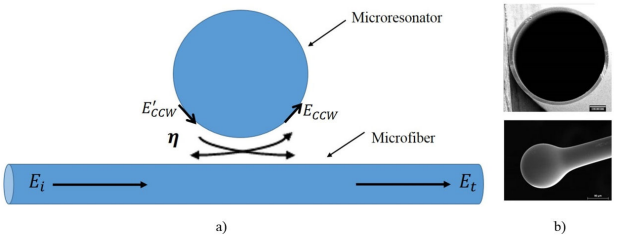

FIGURE 1. a) Scheme of the experimental setup. b) SEM images of two WGM resonators: a microcapillary and a microsphere.

termined by the phase velocity of the WGM and the perimeter of the microresonator cross-section:

$$E'_{ccw} = fe^{-j\phi}E_{ccw}. \tag{2}$$

Combining Eqs. (1) and (2), we obtain the amplitudes of the WGM and the transmitted wave as a function of the input wave:

$$E_{ccw} = \left(\frac{j\eta}{1-\sqrt{1-\eta^2}fe^{-j\phi}}\right), \tag{3}$$

$$E_t = \left(\frac{\sqrt{1-\eta^2}-fe^{-j\phi}}{1-\sqrt{1-\eta^2}fe^{-j\phi}}\right). \tag{4}$$

Finally, we can obtain transmitted power P_t versus the input power P_i computing the amplitude squared of the waves:

$$P_t = \left(1-\frac{\eta^2(1-f^2)}{1+(1-\eta^2)f^2-2\sqrt{1-\eta^2}f\cos(\phi)}\right)P_i. \tag{5}$$

Figure 2 gives a theoretical example: the transmittance Pt/Pi versus the phase ϕ, computed for $\eta = 0.26899$ and $f = 0.95542$. We observe that when $\phi = 0$, *i.e.*, when the WGM adds in phase every round trip, a resonance appears. Figure 2 includes some lines and labels to illustrate the definition of some of the most characteristics parameters: the maximum transmittance level ($T_{\max}$), the minimum at resonance ($T_{\min}$), and the linewidth measured at $T_{1/2} = (T_{\max} + T_{\min})/2$ ($\Delta\phi$ in Fig. 2).

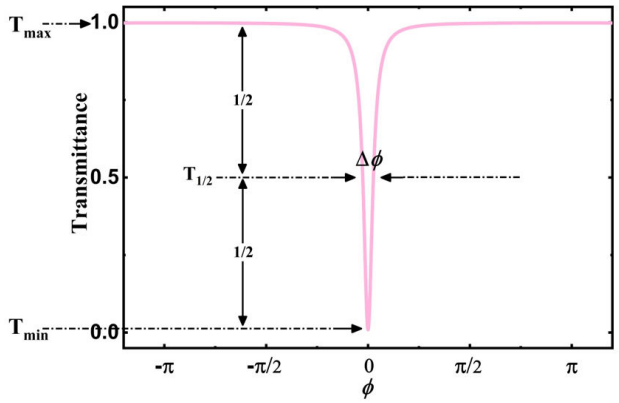

FIGURE 2. Transmittance versus ϕ for a theoretical resonance.

The characteristic parameters $T_{\max}$, $T_{\min}$, and $\Delta\phi$ can be calculated from Eq. (5):

at $\phi = 0$:

$$T_{\min} = \left(1-\frac{\eta^2(1-f^2)}{(1-\sqrt{1-\eta^2}f)^2}\right), \tag{6}$$

at $\phi = 0$:

$$T_{\max} = \left(1-\frac{\eta^2(1-f^2)}{(1+\sqrt{1-\eta^2}f)^2}\right), \tag{7}$$

$$\Delta\phi = 2\cos^{-1}\left(\frac{2\sqrt{1-\eta^2}f}{1+(1-\eta^2)f^2}\right) \cong 2\frac{1-\sqrt{1-\eta^2}f}{\sqrt{\sqrt{1-\eta^2}f}}, \tag{8}$$

where the approximation in Eq. (8) applies for high Q resonances.

From a practical point of view, the transmittance is measured versus wavelength (λ), so it is useful to write the relation between ϕ and λ:

$$\phi = \frac{2\pi}{\lambda}n_m 2\pi a, \tag{9}$$

where n_m is the WGM index and a the microresonator radius. The WGM index is the modal index that is determined by the phase velocity of the surface wave that defines the WGM and propagates along with the interface of the resonator. The actual value of n_m can be obtained by solving Maxwell equations for the specific geometry of the resonator and is slightly lower than the refractive index of the resonator material. For example, in a cylindrical resonator as the one reported in Fig. 3 made of silica, $n_m = 1.398$. Thus, for a high Q resonator, the linewidth in terms of wavelength is given by the expression:

$$\Delta\lambda \cong 2\frac{1-\sqrt{1-\eta^2}f}{\left(\frac{2\pi}{\lambda}\right)^2 n_m a\sqrt{\sqrt{1-\eta^2}f}}. \tag{10}$$

Besides from an experimental point of view, if we measure the transmitted power without normalization, we can quite easily obtain the experimental value for the ratio $P_{t,\min}/P_{t,\max}$. Therefore, it is useful to have the theoretical expression for that ratio:

$$\frac{P_{t,\min}}{P_{t,\max}} \cong \left(\frac{(\sqrt{1-\eta^2}-f)(1+\sqrt{1-\eta^2}f)}{(\sqrt{1-\eta^2}+f)(1-\sqrt{1-\eta^2})}\right)^2. \tag{11}$$

In a typical experiment, after measuring the transmission spectrum around a resonance, we can work out the experimental values for $\Delta\lambda$ and $P_{t,\min}/P_{t,\max}$. Then, using Eqs. (10) and (11) we can compute the actual values of η and f, assuming the radius a is known. As an example, we

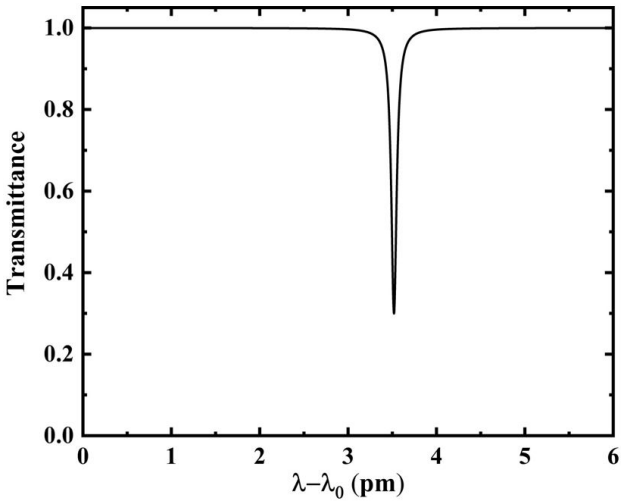

FIGURE 3. Experimental transmittance versus λ, being λ_0 an arbitrary wavelength of reference. The theory matches perfectly this spectrum with: $\eta = 0.004050$ and $f = 0.9999719$.

include in Fig. 3 the experimental transmission spectrum of a WGM resonance ($\lambda = 1529.3$ nm) of a cylindrical resonator that has a radius of 55 μm. The experimental characteristic parameters are: $\Delta\lambda = 0.056$ pm and $P_{t,\min}/P_{t,\max} = 0.30$. Then, we can work out the values of the parameters: $\eta = 0.004050$ and $f = 0.9999719$. The theoretical curve calculated with these values for the coupling coefficient and overall transmission factor matches perfectly the experimental curve with no significant difference.

Once the parameters η and f have been adjusted for a specific resonance, one can exploit the theoretical model to investigate other properties of the resonator as, for example, the amplitude of the WGM propagating in the resonator (see Eq. (3)). From Eq. (11) we can identify an interesting situation: if $\sqrt{1-\eta^2} = f$, then P_t at resonance is zero. The coupling coefficient that accomplishes this condition is named the critical coupling η_c. In the example of Fig. 3, for an overall transmission factor $f = 0.9999719$, the critical coupling is $\eta_c = 0.00750$. In the experiment reported in Fig. 3, the resonator is under coupled ($\eta < \eta_c$), and it should be possible to increase the coupling up to the point of reaching the critical coupling, for example, by decreasing the separation between the microfiber and the resonator o decreasing the radius of the microfiber, in order to increase the amplitude of the evanescent field. In the case of an over-coupled resonance ($\eta > \eta_c$), we should look for a way of reducing the coupling coefficient.

3. The energy balance model (EBM)

In order to introduce the EBM, after the analysis of the system using the WPM, we need to have in mind that high Q resonators will have an overall transmission factor f extremely close to one, so the difference between E'_{ccw} and E_{ccw} will be very small, and a coupling coefficient also very small ($\eta \ll 1$). Similarly, the changes of the amplitudes when going through the coupling region will also be very small. Besides the time that the WGM takes to perform one round trip (τ) will be also extremely small for typical microresonators. Therefore, the ratio between the increment of WGM amplitude per round trip and the τ can be model as the derivative of the WGM amplitude with respect the time. Moreover, at frequencies very close to the frequency of resonance, the phase change per round trip at frequencies slightly out of resonance will also be very small (being exactly zero at resonance). Following Ref. [13], we can write a differential equation for the evolution of the E_{ccw} amplitude with time:

$$\frac{dE_{ccw}}{dt} = -(\kappa_0 + \kappa_1 + j\delta\omega)E_{ccw} + j\frac{\eta}{\tau}E_i. \tag{12}$$

In this equation, κ_0 accounts for the WGM losses in a round trip, κ_1 accounts for the losses between WGM ports in the coupling region, $j\delta\omega$ accounts for the phase change per round trip due to a detuning $\delta\omega$, and δ accounts the power coupled into the resonator from the input wave. Each term of this equation is closely related to the parameters of the BPM. Taking into account Eq. (2), we find:

Losses and phase change per round trip:

$$\frac{\Delta E_{ccw}}{\tau} = \frac{fe^{-j\phi} - 1}{\tau}E_{ccw} \cong -\frac{(1-f) + j\phi}{\tau}E_{ccw},$$
$$\rightarrow \kappa_0 = \frac{1-f}{\tau}, \quad \text{and} \quad \delta\omega = \frac{\phi}{\tau}, \tag{13}$$

where $e^{-j\phi} \cong 1 - j\phi$, and $\phi f \cong \phi$, being $f \cong 1$. Besides we have written the phase in terms of the optical frequency: $\phi = \omega\tau = (\omega_0 + \delta\omega)\tau = \delta\omega\tau$; being $\omega_0\tau$ an integer multiple of 2π, since ω_0 is the frequency of resonance.

According to Eq. (1), when the WGM arrives at the coupling region (E'_{ccw} in Fig. 1) and re-couples into the microresonator (E_{ccw}), the transfer of power determines κ_1:

Transfer of power in the coupler:

$$\frac{\Delta E_{ccw}}{\tau} = \frac{\sqrt{1-\eta^2} - 1}{\tau}E_{ccw}$$
$$\rightarrow \kappa_1 = \frac{1 - \sqrt{1-\eta^2}}{\tau} \cong \frac{\eta^2}{2\tau}. \tag{14}$$

Finally, every round trip the contribution to the WGM amplitude from the input wave (see Eq. (1)) is:

Coupling to the WGM from the input wave:

$$\frac{\Delta E_{ccw}}{\tau} = \frac{j\eta}{\tau}E_{ccw}. \tag{15}$$

Equations (13-15) give the relationship between the BPM and the EBM. We can go one step further, solving Eq. (12) in the stationary regime:

$$\frac{dE_{ccw}}{dt} = 0 \rightarrow E_{ccw} = \frac{j\eta/\tau}{\kappa_0 + \kappa_1 + j\delta\omega}E_i. \tag{16}$$

This equation is equivalent to Eq. (3). One can obtain the amplitude of the transmitted wave E_t –and the transmittance $T = P_t/P_i$ –using Eq. (1). Since the EBM is specifically developed for high Q resonators and the vicinity of resonance, we can neglect all second-order terms (having in mind that the coefficients $\kappa_0\tau, \kappa_1\tau$, $\delta\omega\,\tau$ and η are small):

$$E_t = \left[1 - \frac{2\kappa_1}{\kappa_0 + \kappa_1 + j\delta\omega}\right] E_i,$$

$$T = 1 - \frac{4\kappa_0\kappa_1/(\kappa_0+\kappa_1)^2}{1 + (\delta\omega/[\kappa_0+\kappa_1])^2}. \qquad (17)$$

We can observe that at resonance ($\delta\omega = 0$), if $\kappa_0 = \kappa_1$, then $T = 0$. This result gives the critical coupling condition, discussed in Sec. 2, in terms κ_0 and κ_1. The over-coupling and under coupling situations will correspond to $\kappa_1 > \kappa_0$ and $\kappa_0 > \kappa_1$, respectively. The linewidth of the resonance, as it is defined in Fig. 2, is $\Delta\omega_{1/2} = 2(\kappa_0 + \kappa_1)$, in agreement with Eq. (8).

To conclude this section it is worthwhile to discuss briefly the main advantages of each one of these two models. On the one hand, the BPM can be applied to low Q resonators and gives the transmittance both in the vicinity of the resonance and far away from it. In fact, the BPM describes the whole transmission spectrum and the free spectral range (FSR) of a given family of resonances, provided we write the phase difference as a function of the wavelength, being the FSR determined by the periodicity of the cosine function (see Eqs. (5) and (9)). On the other hand, the EBM can be applied only in the vicinity of a single resonance with a high Q factor. The main advantage that we can point out for the EBM model is the simplicity with which we can describe realistic resonators in which a bunch of physical effects is used to be present simultaneously. For example, different losses mechanism as material absorption, radiation, scattering, and coupling losses can be described correctly adding different κ_i coefficients. In particular, we have found that the EBM is very powerful for the description of the physical effects produced by surface roughness and another mechanism that could couple clockwise and counterclockwise WGM. We dedicate the next section to the analysis of a resonator with coupled counter-propagating WGM.

4. Reflected wave from a WGM resonator

Here we want to model a resonator with coupled counter-propagating WGM, which is a realistic case since surface roughness produces a distributed coupling. Several years ago we reported an analysis of the reflected power in a WGM resonator using a BPM [16]. Such an approach was rather cumbersome and limited. Moreover, it required the assumption of placing in a single point of the resonator an effective reflection coefficient and add up the series of successive reflected and transmitted waves. Here we will apply the EBM, following again the development presented in [13].

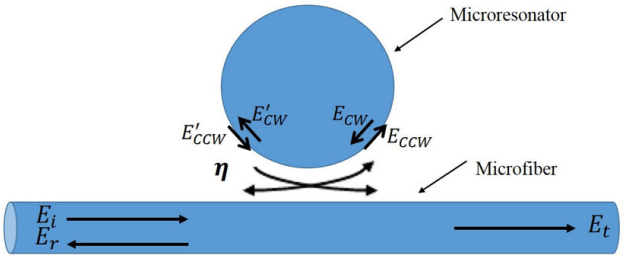

FIGURE 4. Scheme of the experimental setup including the clockwise WGM generated by the coupling between counter-propagating waves.

We model the distributed coupling along the surface of the microresonator as a distributed four ports coupler, similar to Eq. (1), which connects the reflected and transmitted WGM waves with an overall coupling coefficient g. Thus, Eq. (12) has to be modified to include the contribution of g and a new equation for E_{cw} appears (see Fig. 4):

$$\frac{dE_{ccw}}{dt} = -(\kappa_0 + \kappa_1 + j\delta\omega)E_{ccw} + j\frac{\eta}{\tau}E_i + jgE_{cw} \qquad (18)$$

$$\frac{dE_{ccw}}{dt} = -(\kappa_0 + \kappa_1 + j\delta\omega)E_{cw} + jgE_{ccw}. \qquad (19)$$

Thus, in the stationary regime, we can obtain the amplitudes of the counter-propagating waves, E_{ccw} and E_{cw}, and the transmitted and reflected powers, using Eq. (1):

$$T = \frac{(\kappa^2 + g^2 - 2\kappa_1\kappa + \delta\omega^2) + (2\kappa_0\delta\omega)^2}{(2\kappa_1 g)^2 + (\delta\omega^2 + \kappa^2 - g^2)^2}, \qquad (20)$$

$$R = \frac{(2\kappa_1 g)^2}{(2\kappa_1 g)^2 + (\delta\omega^2 + \kappa^2 - g^2)^2} \qquad (21)$$

where $\kappa = \kappa_0 + \kappa_1$. In an ideal system with no losses -*i.e.*, $\kappa_0 = 0$- we can verify that $R + T = 1$. Besides,

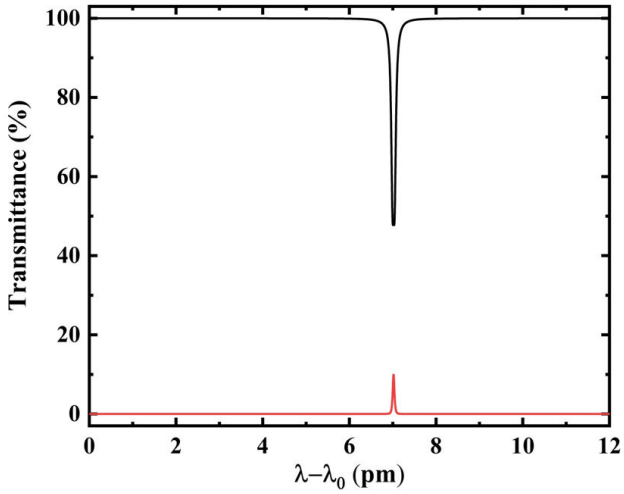

FIGURE 5. Experimental transmittance and reflectance versus λ, being λ_0 an arbitrary wavelength of reference. The theory matches perfectly this spectrum with: $\kappa_0 = 1.97 \times 10^7$ s^{-1}, $\kappa_1 = 1.82\times10^7$ s^{-1}, and $g = 1.52\times10^7$ s^{-1}, or the equivalent parameters: $f = 0.9999673$, $\eta = 7.77\times10^{-3}$ and $r = 2.52\times10^{-5}$, being $r = g\tau$.

an analysis of the denominator shows that if $g > \kappa$, then the resonance splits into two peaks determined by $\delta\omega^2 = g^2 - \kappa^2$. In our experiments, we have not observed such a splitting, so we assume that $\kappa > g$. At resonance -*i.e.*, $\delta\omega = 0$-, we find:

$$R = \left(\frac{2\kappa_1 g}{(\kappa^2 + g^2)}\right)^2,$$
$$T = \left(1 - \frac{2\kappa_1\kappa}{\kappa^2 + g^2}\right)^2 = \left(1 - \frac{\kappa}{g}\sqrt{R}\right)^2. \qquad (22)$$

We can also work out the linewidth of the resonance ($\Delta\omega$) when there is no splitting, using Eq. (21):

$$\Delta\omega = \sqrt{2\sqrt{\kappa^4 + g^4} + g^2 - \kappa^2}. \qquad (23)$$

These equations permit an easy comparison with experimental data. Figure 5 gives an experimental example that corresponds to a resonance of a silica cylinder of 55 μm radius, centered at 1529 nm, with $R = 0.10$ and $T = 0.48$ at resonance and a linewidth of 0.10 pm. From Eq. (22) we obtain $\kappa/g = 2.43$, $\kappa_1/g = 1.20$, $\kappa_0/g = 1.23$, and from Eq. (23) we obtain $g = 1.52\times10^7$ s^{-1}. Thus, $\kappa = 3.69\times10^7$ s^{-1}, $\kappa_1 = 1.82\times10^7$ s^{-1}, $\kappa_0 = 1.97\times10^7$ s^{-1}. Taking into account that the round trip time is $\tau = 1.66$ ps, we can obtain the parameters: $f = 0.9999673$, $\eta = 7.77\times10^{-3}$ and $r = 2.52\times10^{-5}$, being $r = g\tau$, an equivalent reflection coefficient between counter propagating WGM.

5. Conclusion

The comparison of BPM and EBM gives an interesting insight into WGM optical resonators. The theoretical results provide good matching with experiments.

Acknowledgments

In memory of Dr. Evgeny Kuzin, with whom it was always a pleasure to discuss physics and life.

1. I. Villegas, A. Díez, J. L. Cruz, and M. V. Andrés, All-optical tuning of WGM resonances in microspheres made of Er/Yb co-doped optical fiber, *IEEE Photon. Technol. Lett.* **26** (2014) 1534, https://doi.org/10.1109/LPT.2014.2327802.
2. E. Rivera-Pérez, A. Díez, M. V. Andrés, J. L. Cruz, and A. Rodríguez-Cobos, Tunable narrowband fiber laser with feedback based on WGM resonances of a cylindrical microresonator, *Opt. Lett.* **38** (2013) 1636, http://dx.doi.org/10.1364/OL.38.001636.
3. P. Del'Haye, A. Schliesser, O. Arcizet, T. Wilken, R. Holzwarth, and T. J. Kippenberg, Optical frequency comb generation from a monolithic microresonator, *Nature* **450** (2007) 1214, http://doi.org/10.1038/nature06401.
4. V. Zamora, A. Díez, M. V. Andrés, and B. Gimeno, Refractometric sensor based on whispering-gallery modes of thin capillaries, *Opt. Express* **15** (2007) 12011, https://doi.org/10.1364/OE.15.012011.
5. E. Rivera-Pérez, I. L. Villegas, A. Díez, M. V. Andrés, J. L. Cruz, and A. Rodríguez-Cobos, Measurement of Pump-Induced Temperature Increase in Doped Fibers Using Whispering-Gallery Modes, *IEEE Photon. Technol. Lett.* **25** (2013) 2498, http://dx.doi.org/10.1109/LPT.2013.2288865.
6. M. Sumetsky and Y. Dulashko, Radius variation of optical fibers with angstrom accuracy, *Opt. Lett.* **35** (2010) 4006, https://doi.org/10.1364/OL.35.004006.
7. T. A. Birks, J. C. Knight, and T. E. Dimmick, High-resolution measurement of the fiber diameter variations using whispering gallery modes and no optical alignment, *IEEE Photon. Technol. Lett.* **12** (2000) 182, https://doi.org/10.1109/68.823510.
8. X. Roselló-Mechó, M. Delgado-Pinar, J. L. Cruz, A. Díez, and M. V. Andrés, Measurement of UV-induced absorption and scattering losses in photosensitive fibers, *Opt. Lett.* **43** (2018) 2897, http://dx.doi.org/10.1364/OL.43.002897.
9. X. Roselló-Mechó, M. Delgado-Pinar, A. Díez, and M. V. Andrés, Measurement of Pockels' coefficients and demonstration of the anisotropy of the elasto-optic effect in optical fibers under axial strain, *Opt. Lett.* **13** (2016) 2934, http://dx.doi.org/10.1364/OL.41.002934.
10. R. I. Álvarez-Tamayo *et al.*, Theoretical and experimental analysis of tunable Sagnac high-birefringence loop filter for dual-wavelength laser application, *Appl. Opt.* **50** (2011) 253, https://doi.org/10.1364/AO.50.000253.
11. O. Duhem, J.F. Henninot, and M. Douay, Study of in fiber Mach-Zehnder interferometer based on two spaced 3-dB long period gratings surrounded by a refractive index higher than that of silica, *Opt. Commun.* **180** (2000) 255, https://doi.org/10.1016/S0030-4018(00)00709-4.
12. M.V. Andrés, and K.W.H. Foulds, Optical-fiber resonant rings based on polarization-dependent cou-plers, *J. Lightwave Technol.* **8** (1990) 1212, https://doi.org/10.1109/50.57843.
13. C. L. Zou *et al.*, Taper-microsphere coupling with numerical calculation of coupled-mode theory, *J. Opt. Soc. Am. B* **25** (2008) 1895, https://doi.org/10.1364/JOSAB.25.001895.
14. G. C. Righini *et al.*, , Whispering gallery mode microresonators: Fundamentals and applications, *Riv. Nuovo Cimento* **34** (2011) 435, http://dx.doi.org/10.1393/ncr/i2011-10067-2.
15. A. V. Kir'yanov, V. N. Filippov, and A. N. Starodumov, Cw-pumped erbium-doped fiber laser passively Q switched with Co21:ZnSe crystal: modeling and experimental study, *Opt. Soc. Am. B* **353** (2002) 353, https://doi.org/10.1364/ASSL.2001.TuA6.

16. V. Zamora, A. Díez, M.V. Andrés, and B. Gimeno, Interrogation of whispering-gallery modes resonances in cylindrical microcavities by backreflection detection, *Opt. Lett.* **34** (2009) 1039, https://doi.org/10.1364/OL.34.001039.